

# Wireless Energy-On-Demand Using Magnetic Quasi-Resonant Coupling

Wei Liu , *Student Member, IEEE*, K.T. Chau , *Fellow, IEEE*, Christopher H.T. Lee , *Senior Member, IEEE*, Chaoqiang Jiang , *Member, IEEE*, Wei Han , *Student Member, IEEE*, and W. H. Lam , *Senior Member, IEEE*

**Abstract**—This article proposes and implements a novel magnetic quasi-resonant coupling (MQRC) scheme to realize the concept of energy-on-demand wireless power transfer (WPT). To prevent illegal receivers harvesting wireless energy, the proposed energy-on-demand technology nominates the authorized receiver to take over the initiative and generate a well-defended security key based on a two-dimensional frequency-and-duration chaos. The switched-capacitorless quasi-resonant transmitter flexibly employs a new continuous operating frequency regulation strategy to self-adapt the arbitrary energy-on-demand from the authorized receiver, hence achieving synchronous multifrequency WPT. Moreover, the proposed MQRC-WPT system takes the merit of power transmission enhancement over conventional one while improving the transmission efficiency especially during low power level. Theoretical analysis, electromagnetic simulation, and practical experimentation are provided to verify the feasibility of proposed energy-on-demand MQRC-WPT system with security.

**Index Terms**—Energy-on-demand, frequency-and-duration chaos, magnetic quasi-resonant coupling (MQRC), wireless energy security.

## I. INTRODUCTION

**D**UE to cleanliness, convenience, and high efficiency, wireless power transfer (WPT) technology has been extensively investigated in various application fields, such as electric vehicle wireless charging [1]–[4], wireless motor [5], and wireless lighting [6]. Especially with multiple receivers, the wireless charging technology can totally eliminate the messy wires, effectively minimize battery packs, and conveniently achieve one-to-many charging environment [7]. Also, this WPT technology will promisingly penetrate various renewable energies into traditional usage patterns of energy.

Manuscript received October 17, 2019; revised January 24, 2020; accepted February 7, 2020. Date of publication February 12, 2020; date of current version May 1, 2020. This work was supported by the Hong Kong Research Grants Council, Hong Kong Special Administrative Region, China, under Project 17204317. Recommended for publication by Associate Editor M. Vitelli. (*Corresponding author: K. T. Chau.*)

Wei Liu, K.T. Chau, Wei Han, and W. H. Lam are with the Department of Electrical and Electronic Engineering, The University of Hong Kong, Hong Kong (e-mail: liuwei@eee.hku.hk; ktchau@eee.hku.hk; weihan@eee.hku.hk; whlam@eee.hku.hk).

Christopher H.T. Lee is with the School of Electrical and Electronic Engineering, Nanyang Technological University, Singapore 639798, Singapore (e-mail: chtlee@ntu.edu.sg).

Chaoqiang Jiang is with the Department of Engineering, The University of Cambridge, CB2 1TN Cambridge, U.K. (e-mail: cj426@cam.ac.uk).

Color versions of one or more of the figures in this article are available online at <http://ieeexplore.ieee.org>.

Digital Object Identifier 10.1109/TPEL.2020.2973408

Generally, the epoch-making WPT consists of the far-field and near-field transmissions. In the former case, many researchers have respectively investigated the acoustic, optical, and microwave schemes for delivering wireless energy and made fruitful achievements. On the other hand, the near-field transmission commonly employs inductive, capacitive, and magnetic resonant coupling (MRC) techniques for WPT. Recently, the MRC-based WPT scheme has been deeply investigated and widely applied [8]. Nevertheless, the security consideration during WPT, namely wireless energy stolen by unauthorized receivers triggers further development of both the far-field and near-field transmission technologies.

Recently, the concept of wireless energy encryption [9] or selective WPT was proposed to promote the development of intelligent transportation. However, this MRC-based energy encryption scheme suffers from low regulation flexibility and poor self-adaptivity. To improve its regulation flexibility and adaptivity, a transistor-controlled variable capacitor has been proposed [10], but its efficiency and power level remain to be raised further. Due to the high operating frequency in this MRC-WPT system, the use of virtual capacitors [11] or electric springs [12] as a potential solution may pose new challenges of the ultrahigh frequency switching and high-speed processing. Besides, the multifrequency superposition methodology [13] and multifrequency programmable pulsewidth modulation strategy [14] were demonstrated to improve compatibility and achieve high efficiency with desired power distributions for multiload MRC-WPT. However, the requirement of multiple inverters or resonant circuits inevitably increases their system and control complexity. Meanwhile, a scheme that uses the fundamental and 3rd harmonic was reported to implement double-frequency WPT [15], but it awaited improvement considering variable-frequency multistandard WPT.

For guaranteeing wireless energy security, the concept of wireless energy encryption was proposed with a 1-D frequency chaos generated by the transmitter [9]. Actually, the wireless energy should be encrypted based on the practical requirements of multistandard receivers rather than the transmitter. Incorporating with a 2-D frequency-and-duration chaos (2-D FDC), a novel concept of wireless energy-on-demand is proposed and implemented to realize simultaneous multistandard WPT in this article, thus fundamentally improving the wireless energy compatibility and security performance. In contrast to the energy-encrypted SF-WPT scheme, the proposed energy-on-demand scheme essentially nominates the authorized receiver

to take over the initiative from the transmitter. Hence, the urgent priority is designing a versatile transmitter to self-adapt the arbitrary energy-on-demand from the authorized receiver. Although a switched-capacitorless transmitter with fixed coil inductance and matched capacitance was identified to exhibit a good selectivity in the MRC-WPT system [16], the transmitter unfortunately operates at nonresonance, especially for energizing diverse receivers. Recently, a quadruple-resonant inverter has been investigated [17], but the number of resonant components can be further reduced for WPT applications. Thus, this mechanism can be extended to newly design a quasi-resonant transmitter for flexible frequency regulation. Consequently, a magnetic quasi-resonant coupling (MQRC) scheme with multiple diverse receivers will be developed to realize energy-on-demand WPT. The concept of MRC is to emphasize the coupling of magnetic resonance between the transmitter and receiver. The magnetic field resonance works as the carrier of energy, thus wirelessly transferring the energy to the receiver. Since the quasi-resonant transmitter operates at quasi-resonance, the generated magnetic field is also quasi-resonance at the transmitter side. Accordingly, the MQRC is derived from the concept of MRC.

To avoid the new critical risk of wireless energy theft, this article contributes to an initiative 2-D chaotic energy-on-demand scheme. In the proposed scheme, a variable capacitor awaits to be developed for dynamic capacitance control at the receiver side. For realizing the dynamic 2-D FDC energy-on-demand, the switched-capacitor array can be readily used to achieve dynamic capacitance adjustment. Differing from the on-demand power control, the proposed energy-on-demand scheme transfers the initiative to the authorized receiver to generate chaotic security keys. The customized requests of dynamically real-time varying operating frequency for the encrypted energy-on-demand can prevent illegal frequency tracking. Working like a broadcaster, the transmitter should satisfy these dynamic requests. With a simultaneous adjustment, the transmitter and authorized receiver can readily encrypt and decrypt the energy packages, respectively.

Section II will discuss the topology and operating principle of the proposed energy-on-demand MQRC-WPT system. Then, Section III will present the energy-on-demand scheme which incorporates a 2-D FDC to enhance security consideration. In Section IV, both simulation and experimental results will be given to verify the proposed system. Finally, the conclusion will be drawn in Section V.

## II. MAGNETIC QUASI-RESONANT COUPLING WIRELESS POWER TRANSFER

The proposed energy-on-demand MQRC-WPT system is depicted in Fig. 1, which mainly comprises one flexible switched-capacitorless quasi-resonant transmitter and multiple receivers, including the authorized and unauthorized ones. To self-adapt the arbitrary energy-on-demand from the authorized receiver, a switched-capacitorless quasi-resonant transmitter is proposed in this system, which can continuously and flexibly attune the operating frequency and its active duration to synchronize the arbitrary energy-on-demand within an encryption range.

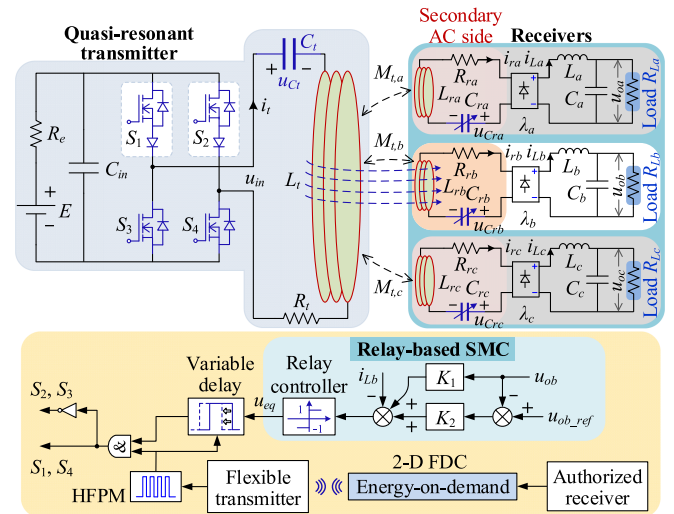


Fig. 1. Proposed energy-on-demand MQRC-WPT system using a switched-capacitorless quasi-resonant transmitter.

The switched-capacitor transmitter inevitably includes a bulky switched-capacitor array, which is composed of bidirectional switches and a capacitor array, to adjust the compensated capacitance discretely and thus the corresponding resonant frequency for selective WPT [5] or variable-frequency WPT [9]. The proposed transmitter only uses a fixed capacitor rather than a switched-capacitor array for variable multifrequency WPT (MF-WPT). Taking over the initiative of energy-on-demand, the authorized receiver will generate the 2-D FDC as security keys. The information interaction can secretly deliver the security keys to the transmitter via wireless communication. Then, the high-frequency pulse modulation (HFPM) will change its frequency to synchronize the energy-on-demand. A relay-based sliding mode control (SMC) is introduced as an alternative control scheme to stabilize the output voltage at different frequencies. The relay controller generates the control logic and the variable-time delay serves to guarantee the completion of current switching half-cycle [17]. As a rapid pulse density modulation, the relay-based SMC can incorporate with the HFPM to control the inverter switches.

The key of quasi-resonant transmitter is to artfully split the positive and negative half-cycles of the sinusoidal resonant current, and artificially inject a dead zone between these two half-cycles, thus creating flexible frequency variability for the desired energy-on-demand WPT. Meanwhile, the proposed scheme contributes to a quasi-resonance operation even at inconsistent resonant frequencies between the transmitter and the authorized receiver. The switched-capacitor MRC-WPT mainly suffers from discrete frequency regulation and finite selections, which fails to operate at the arbitrary energy-on-demand frequency. Conversely, the proposed MQRC-WPT takes the merits of eliminating the transmitter's switched-capacitor array, continuously regulating the operating frequency within an encryption range, and maintaining quasi-resonant operation with a fixed transmitter's capacitor.

The quasi-resonant transmitter only employs an H-bridge inverter using power devices without antiparallel diodes. This unidirectional H-bridge inverter can readily achieve the target of splitting positive and negative resonant half cycles and then inject an adjustable dead zone without using any extra switching devices or auxiliary circuit. For better utilization of power devices with antiparallel body diodes, an alternative scheme that is derived from the conventional H-bridge inverter is realized by concatenating one diode in each of its upper legs, as shown in Fig. 1. The transmitter resonant current is forced to flow unidirectionally through switches  $S_1$  and  $S_4$  (or  $S_2$  and  $S_3$ ) while maintaining the applicability of various control strategies. In Fig. 1, an ideal variable capacitor is employed in each potentially authorized receiver. Practically, a switched-capacitor array, as an effective capacitance adjustment, can be used to implement the secondary variable capacitor according to the dynamic energy-on-demand with the 2-D FDC, thus dynamically adjusting the matched capacitance. With different energy requests, the transmitter should be competent for operating at a variable frequency in a continuous way by varying the dead zone rather than in a discrete way via selective switched-capacitor arrays. The inverter with connecting diodes [18] contributes to a quasi-resonant operation even if the operating frequency chaotically varies, thus satisfying the arbitrary energy-on-demand and improving multistandard WPT compatibility while maintaining wireless energy security.

### A. Operating Principle

In Fig. 1,  $R_e$  is the internal resistance of power source  $E$ . Denotations  $R_t$ ,  $L_t$ ,  $C_t$ ,  $i_t$ ,  $u_{Ct}$ ,  $R_{rk}$ ,  $L_{rk}$ ,  $C_{rk}$ ,  $i_{rk}$  and  $u_{Crk}$  ( $k \in \{a, b, c\}$ ) with subscripts  $t$  and  $r$  denote the coil internal resistances, resonant coil inductances, matched capacitances, resonant currents, and resonant voltages of the transmitter and receiver circuits in the  $k$ th WPT channel, respectively. Denotation  $u_{ok}$  is the output voltage of the  $k$ th receiver. Meanwhile,  $M_{t,k}$  denotes the mutual inductance between the transmitter and each receiver coils, while  $M_{rk1,k2}$  is that between each two receiver coils. Also,  $\lambda_k$  obeys a random distribution, which represents the number of receivers in the  $k$ th energy-on-demand channel.

To commence with theoretical analysis, some assumptions are made as follows: 1)  $M_{t,k} \gg M_{rk1,k2}$ , and  $M_{rk1,k2}$  is negligible, 2)  $Z_{Lk\_eq}$  and  $R_{Lk\_eq}$  are the equivalent impedance and resistance at the secondary ac side, 3)  $u_{Ct}(t_{0-})$  denotes the initial voltage through  $C_t$  at the beginning of the switching period  $T_1$ , and  $i_{t\_eq}$  is the equivalent fundamental current of  $i_t$ . In the following analysis, the  $b$ th group of receivers is assumed to be authorized. The operation can fall into the following three modes, where *Mode 1* involves a positive half-cycle resonance (*Stage 1*) and a tunable dead zone (*Stage 2*); *Mode 2* involves a negative half-cycle resonance (*Stage 1*) and a tunable dead zone (*Stage 2*); and *Mode 3* is an idle state, in which all switches are turned OFF.

*Mode 1 Stage 1* [0,  $T/2$ ]: As depicted in Fig. 2(a),  $S_1$  and  $S_4$  are turned ON while  $S_2$  and  $S_3$  are OFF so that the positive half-cycle resonance of  $L_t$  and  $C_t$  occurs. By using the Laplace transform, the key operating parameters in the frequency domain can be

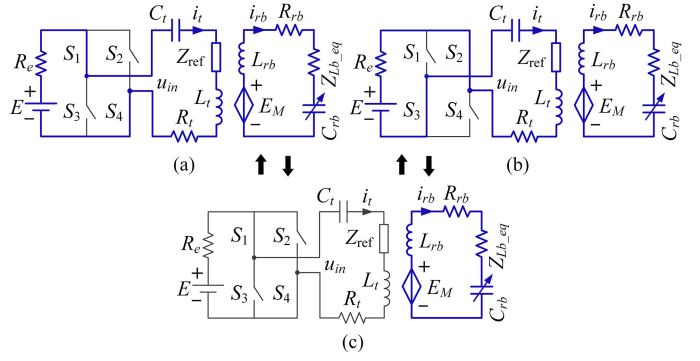


Fig. 2. Operating modes in one switching cycle. (a) *Mode 1 Stage 1*. (b) *Mode 2 Stage 1*. (c) *Mode 1 Stage 2*, *Mode 2 Stage 2*, and *Mode 3*.

expressed as

$$\begin{cases} i_t(s) = \frac{E/s - u_{Ct}(t_{0-})/s}{Z_{ref} + (R_e + R_t) + sL_t + 1/C_t s} \\ u_{Ct}(s) = \left[ \frac{E}{s} - \frac{u_{Ct}(t_{0-})}{s} \right] \frac{1/C_t s}{Z_{ref} + (R_e + R_t) + sL_t + 1/C_t s} \end{cases} \quad (1)$$

where  $s$  is a complex frequency parameter  $s = \sigma + j\omega$ , with real numbers  $\sigma$  and  $\omega$ . At the transmitter side, the total impedance  $Z_{ref}$  reflected from all relevant receiver circuits and the  $k$ th impedance  $Z_{refk}$  reflected from the  $k$ th receiver circuit can be written as

$$\begin{aligned} Z_{ref} &= \sum_{k \in \{a, c\}} (\lambda_k Z_{refk}) + \frac{\lambda_b (\omega_b M_{t,b})^2}{R_{rb} + Z_{Lb\_eq}} \\ Z_{refk} &= \frac{(\omega_b M_{t,k})^2}{Z_{rk}} \end{aligned} \quad (2)$$

where  $Z_{rk}$  and  $\omega_b$  are the  $k$ th receiver's self-impedance and energy-on-demand angular frequency, respectively. Since the  $b$ th group of receivers is authorized to conduct wireless energy-on-demand, all the receivers will operate at the resonant angular frequency  $\omega_b$  rather than their respective innate resonant ones  $\omega_k$ . The authorized  $b$ th receivers operate at resonance with a lower self-impedance  $Z_{rb} = R_{rb} + Z_{Lb\_eq}$ , while the unauthorized  $a$ th or  $c$ th receivers operate at nonresonance with a larger self-impedance  $Z_{rk} = R_{rk} + Z_{Lk\_eq} + j\omega_b L_{rk} + 1/(j\omega_b C_{rk})$ , where  $k \in \{a, c\}$ . Consequently, (1) can be solved as

$$\begin{cases} i_t(t) = [E - u_{Ct}(t_{0-})] / (\omega_t L_t) e^{-\alpha t} \sin \left( \sqrt{1 - (\alpha/\omega_t)^2} \omega_t t \right) \\ u_{Ct}(t) = E - [E - u_{Ct}(t_{0-})] e^{-\alpha t} \cos \left( \sqrt{1 - (\alpha/\omega_t)^2} \omega_t t \right) \end{cases} \quad (3)$$

where  $\omega_t = 1/\sqrt{L_t C_t}$  and  $\alpha = (Z_{ref} + R_e + R_t)/(2L_t)$ . Since  $R_e$ ,  $R_t$ ,  $Z_{refa}$  and  $Z_{refc}$  from unauthorized receivers are far lower than  $Z_{refb}$  from the authorized receivers,  $\alpha/\omega_t$  can be simplified as

$$\alpha/\omega_t \simeq \frac{\lambda_b (\omega_b M_{t,b})^2}{2L_t \omega_t (R_{rb} + Z_{Lb\_eq})} = \frac{\lambda_b \omega_b M_{t,b}}{2(R_{rb} + Z_{Lb\_eq})} \left( \frac{M_{t,b}}{L_t} \frac{\omega_b}{\omega_t} \right) \quad (4)$$

where  $\omega_b \leq \omega_t$ ,  $M_{t,b}/L_t \leq k_c$ , and  $k_c$  is the coupling coefficient. In a weak coupling WPT system,  $\alpha/\omega_t < 1$

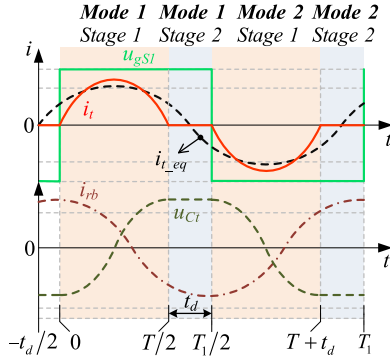


Fig. 3. Theoretical waveforms of MQRC-WPT.

and  $(\alpha/\omega_t)^2 \ll 1$  can be obtained within the range of  $\lambda_b \omega_b M_{t,b} / [2(R_{rb} + Z_{Lb_{eq}})] < 1/k_c$  since  $M_{t,b} \omega_b / (L_t \omega_t) \leq k_c$ . Due to  $(\alpha/\omega_t)^2 \ll 1$ , the transmitter's actual resonant frequency can be written as  $\omega = \omega_t \sqrt{1 - (\alpha/\omega_t)^2} \simeq \omega_t$ , where  $\omega_t = 2\pi/T$ . Taking into account various practical parameter variations, the operation characteristics are still dominantly determined by the influence of authorized *b*th receivers rather than that of unauthorized ones. No matter in stationary or dynamic WPT systems, these characteristics exhibit good tolerance. This insignificant frequency deviation will contribute to a quasi-resonant operation. Moreover, this so-called MQRC-WPT inherently permits the transmitter and authorized receiver to operate at different frequencies, which differs from the same-frequency resonance in the MRC-WPT. Since  $e^{-\alpha t}$  can be regarded as unity ( $-\alpha t \simeq 0$ ) in (3) during the super-short resonant half-cycle, it has no effect on the proposed quasi-resonant operation. Both  $i_t$  and  $u_{Ct}$  across  $C_t$  are approximately in a form of half-cycle sinusoid with an angular frequency  $\omega_t$  as depicted in Fig. 3. Their peak values at  $t = T/4$  and  $t = T/2$ , namely  $i_{tm}$  and  $u_{Ctm}$ , can be approximated by

$$\begin{cases} i_{tm} \simeq (E + u_{Ctm}) / (L_t \omega_t) e^{-\pi \sqrt{C_t/L_t} (Z_{ref} + R_e + R_t)/4} \\ u_{Ctm} \simeq E \left[ 1 + e^{-\pi \sqrt{C_t/L_t} (Z_{ref} + R_e + R_t)/2} \right] / e^{-\pi \sqrt{C_t/L_t} (Z_{ref} + R_e + R_t)/2}. \end{cases} \quad (5)$$

Hence,  $i_{tm}$  and  $u_{Ctm}$  as well as the transmitted power increase with the increasing  $C_t$  and the decreasing  $L_t$ , and vice versa. In Fig. 3,  $u_{gS1}$  is the gate signal of switch  $S_1$ ;  $t_d$  is the controllable dead zone time between the positive and negative resonant half-cycles;  $T$  and  $\omega$  are the innate resonant period and the angular frequency of transmitter circuit, respectively; and  $T_1$  is the switching period of gate signal.

**Mode 1 Stage 2** [ $T/2, T_1/2$ ]: In Fig. 2(c), the positive half-cycle resonance has finished and all switches are turned OFF. The transmitter current  $i_t$  is zero and the voltage  $u_{Ct}$  keeps constant, as shown in Fig. 3, whereas  $i_{rb}$  continuously freewheels in the authorized receiver. Thus, it yields

$$i_t(t) = 0, \quad u_{Ct}(t) = u_{Ctm} = -u_{Ct}(t_{0-}). \quad (6)$$

**Mode 2 Stage 1** [ $T_1/2, T + t_d$ ]: In Fig. 2(b),  $S_1$  and  $S_4$  are turned OFF while  $S_2$  and  $S_3$  are ON so that the negative half-cycle

resonance of  $L_t$  and  $C_t$  occurs. Its analysis is correspondingly the same as *Stage 1, Mode 1*. The parameters can be derived as

$$\begin{cases} i_t(t) = [-E + u_{Ct}(t_{0-})] / (\omega_t L_t) e^{-\alpha t} \sin(\omega(t - T_1/2)) \\ u_{Ct}(t) = -E - [-E + u_{Ct}(t_{0-})] e^{-\alpha t} \cos(\omega(t - T_1/2)) \end{cases} \quad (7)$$

where  $\omega = \omega_t \sqrt{1 - (\alpha/\omega_t)^2} \simeq \omega_t$ . Their negative peak values  $-i_{tm}$  and  $-u_{Ctm}$  occur at  $t = T_1/2 + T/4$  and  $t = T + t_d$ , respectively.

**Mode 2 Stage 2** [ $T + t_d, T_1$ ]: In Fig. 2(c), the negative half-cycle resonance has finished. Its analysis is correspondingly the same as *Stage 2 in Mode 1*. Thus, both  $i_t$  and  $u_{Ct}$  are in a form of half-cycle sinusoid in *Stage 1*, and then keep zero and constant in *Stage 2*, respectively. Thus, it yields

$$i_t(t) = 0, \quad u_{Ct}(t) = -u_{Ctm} = u_{Ct}(t_{0-}). \quad (8)$$

**Mode 3**: As depicted in Fig. 2(c), all switches are OFF. Thus,  $i_{rb}$  continuously freewheels and gradually decays until the next switching cycle. Since all switches can be turned OFF alternatively at  $t_{off} = T_1/2$  or  $t_{off} = T_1$  as shown in Fig. 3, it yields

$$i_t(t) = 0, \quad \begin{cases} u_{Ct}(t)_{t_{off}=T_1/2} = u_{Ctm} = -u_{Ct}(t_{0-}) \\ u_{Ct}(t)_{t_{off}=T_1} = -u_{Ctm} = u_{Ct}(t_{0-}). \end{cases} \quad (9)$$

The discontinuous current operations occur at *Mode 1 Stage 2, Mode 2 Stage 2, and Mode 3*. It can be used for proportionally adjusting the fundamental and 3rd harmonic components, and thus contributes to variable-frequency multistandard WPT for the arbitrary energy-on-demand. In Fig. 3, no matter the switch  $S_1$  is being turned ON or turned OFF, the transmitter current  $i_t$  already becomes zero. Thus, the switched-capacitorless quasi-resonant transmitter can theoretically achieve zero-current-switching (ZCS) operation [17], [19]. Practically, the output capacitances of nonideal power devices may slightly degrade the ZCS operation. As a crucial risk of energy security in multiobjective WPT applications, energy stealing will cause severe energy leakage and significantly reduce the system efficiency. Due to the oscillation frequency invariance, the injection of a tunable dead zone can be realized by adjusting the switching frequency in a discontinuous current mode. By only regulating the switching frequency and its duration, the proposed switched-capacitorless quasi-resonant transmitter can flexibly attune both the equivalent operating frequency and its active duration to synchronize the chaotic energy-on-demand ones.

## B. Power Transmission Enhancement

After the rectification, a tiny inductive impedance will be introduced into the secondary ac side [5]. A smoothing inductor  $L_b$  is predesigned in such a way that the output impedance  $Z_{Lb}$  can be expressed as

$$\begin{aligned} Z_{Lb} &= j\omega_{high} L_b \delta + 1 / (j\omega_{low} C_b + 1/R_{Lb}) \\ &\simeq j\omega_{high} L_b \delta + R_{Lb} \end{aligned} \quad (10)$$

where  $\omega_{low} \simeq 0$ ,  $\omega_{high}$  is the oscillation angular frequency of the inductor current, and  $\delta$  is the ratio of the ac root-mean-square value to dc inductor current. Accordingly, the amplitude of  $Z_{Lb}$

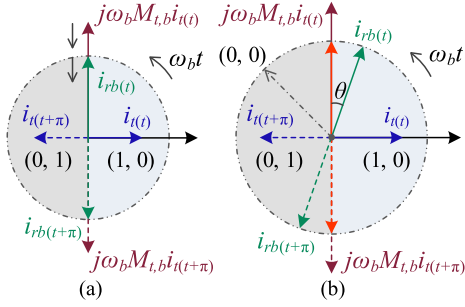


Fig. 4. Phasor diagrams. (a) MRC scheme. (b) MQRC scheme.

with the inductor  $L_b$  is larger than that without the inductor  $L_b$ . From (2), the amplitude of  $Z_{ref}$  in the proposed scheme is lower than that in the conventional one. As compared with the conventional scheme, the proposed one essentially enlarges the transmitter current  $i_t$ , as depicted in Fig. 4, which can then enhance the mutually induced electromotive force (EMF)  $j\omega_b M_{t,b} i_t$ . Because of the steady-state volt-second balance of  $L_b$ , the enhanced  $j\omega_b M_{t,b} i_t$  can produce higher load current and hence higher receiving power. Since the increasing  $L_b$  will contribute to a further lower  $Z_{ref}$  and thus larger  $i_t$ , both the EMF and the receiving power will be further enlarged.

Moreover, the conventional scheme operates at continuous current mode and involves only two current vectors (0, 1) and (1, 0), as shown in Fig. 4(a), where the value “1” or “0” represents that the upper leg in the H-bridge inverter is ON or OFF, respectively. When the vector (0, 1) switches to (1, 0), a negative EMF  $j\omega_b M_{t,b} i_{t(t+\pi)}$  is induced to prevent the projection value of  $i_{rb(t)}$  further increasing along the vertical axis. Hence, the projection value will first decrease from  $i_{rb(t)}$  and then inversely increase to  $i_{rb(t+\pi)}$ . In contrast, the proposed quasi-resonant scheme operates at discontinuous current mode and involves three current vectors including the zero-current vector (0, 0), as depicted in Fig. 4(b). Since  $Z_{Lb}$  is an inductive impedance,  $i_{rb}$  lags behind  $j\omega_b M_{t,b} i_t$  by an angle  $\theta$ . First, the vector (0, 1) switches to (0, 0) instead of (1, 0), thus both  $i_{t(t)}$  and  $j\omega_b M_{t,b} i_{t(t)}$  decay to zero. Meanwhile,  $i_{rb(t)}$  freewheels and keeps resonant freely, which leads to an increasing projection value along the vertical axis, further larger than that in the conventional scheme. Second, when the vector (0, 0) switches to (1, 0), a negative  $j\omega_b M_{t,b} i_{t(t+\pi)}$  is induced to counteract  $i_{rb}$ . The projection value will first decrease and then inversely increase to  $i_{rb(t+\pi)}$ . Thus, the proposed scheme effectively achieves power transmission enhancement.

### C. Multifrequency WPT

When the dead zone time  $t_d > 0$ , the discontinuous half-cycle resonant transmitter current can be expressed as a Fourier series

$$i_t(t_1) = A \cdot \sum_{n=1}^{\infty} \left[ \frac{(-1)^{(n-1)} \cos(N\omega_b T/4)}{\omega^2 - (N\omega_b)^2} \sin(N\omega_b t_1) \right], n \in \mathbb{Z}^+ \quad (11)$$

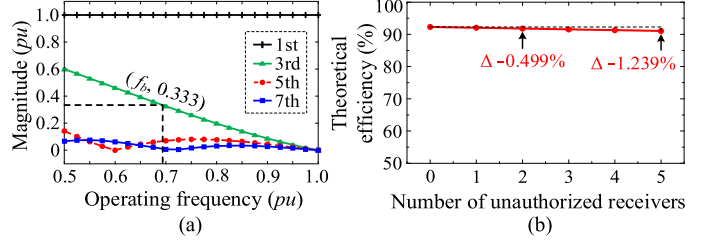


Fig. 5. System characteristics of proposed quasi-resonant inverter. (a) Variation of magnitudes. (b) Variation of efficiencies.

where  $A = 8i_{tm}\omega/T_1$ ,  $N = 2n-1$  and  $t_1 = t-t_d/2$ , which contains only the fundamental and odd-harmonic components. Also,  $\omega_b$  will decrease with the increasing  $t_d$ , and thus the percentage of 3rd harmonic will increase with  $t_d$ . Fig. 5(a) shows the normalized magnitudes of the 1st, 3rd, 5th, and 7th harmonics. Considering the secondary EMF that is proportional to the operating frequency, the 1st and 3rd harmonics can be used for high-power WPT, while the 5th and 7th harmonics for relatively low-power WPT. By utilizing the fundamental component, the single-frequency WPT (SF-WPT) can only transmit single-frequency wireless power to specific receivers at one moment. By simultaneously using the 1st and 3rd harmonic components, the MF-WPT can improve the compatibility for powering different receivers, especially with different power levels. When the energy-on-demand scheme selects different frequencies with different percentages of the 3rd harmonic, the power distribution among different authorized receivers can be artificially regulated. Although with relatively low magnitudes, the orders of the 5th and 7th harmonics are five and seven times larger than that of the fundamental one. Thus, they can be used for low-power wireless charging with a relatively long transfer distance.

When the  $b$ th group of receivers is authorized, both the transmitter and the  $b$ th authorized receivers operate at their respective inherent resonances. In either SF-WPT or MF-WPT operation, the general equation [14] can be derived as

$$\begin{bmatrix} Z_t & Z_{t,a}^{(i)}\lambda_a & Z_{t,b}^{(i)}\lambda_b & Z_{t,c}^{(i)}\lambda_c \\ Z_{t,a}^{(i)} & Z_{ra}^{(i)} & Z_{ra,b}^{(i)}\lambda_b & Z_{ra,c}^{(i)}\lambda_c \\ Z_{t,b}^{(i)} & Z_{ra,b}^{(i)}\lambda_a & Z_{rb}^{(i)} & Z_{rb,c}^{(i)}\lambda_c \\ Z_{t,c}^{(i)} & Z_{ra,c}^{(i)}\lambda_a & Z_{rb,c}^{(i)}\lambda_b & Z_{rc}^{(i)} \end{bmatrix} \begin{bmatrix} i_{ta}^{(i)} \\ i_{tb}^{(i)} \\ i_{tc}^{(i)} \end{bmatrix} = \begin{bmatrix} U_{in}^{(i)} \\ 0 \\ 0 \end{bmatrix} \quad (12)$$

where  $Z_{t,k}^{(i)} = j\omega_b^{(i)} M_{t,k}$  and  $Z_{rk1,k2}^{(i)} = j\omega_b^{(i)} M_{rk1,k2}$ . The superscript  $(i)$  represents the selected 1st or 3rd harmonic;  $U_{in}^{(i)}$  is the root-mean-square value of input voltage  $u_{in}$ ; and  $Z_t$  and  $Z_{rk}^{(i)}$  denote the impedances of the transmitter and  $k$ th receiver circuits, respectively. They can be expressed as

$$\begin{cases} Z_t = R_t + j\omega_t L_t + 1/(j\omega_t C_t) = R_t \\ Z_{rk}^{(i)} = Z_{Lk_{eq}} + R_{rk} + j\omega_b^{(i)} L_{rk} + 1/(j\omega_b^{(i)} C_{rk}). \end{cases} \quad (13)$$

If the  $a$ th group of receivers is simultaneously authorized to pick up the 3rd harmonic wireless power, there are



TABLE I  
DESIGN SPECIFICATIONS AND PARAMETERS

Items	Value
DC bus voltage ( $E$ )	40 V
Transmitter coil turns ( $n_t$ )	24
Transmitter capacitance ( $C_t$ )	5.50 nF
Transmitter coil inductance ( $L_t$ )	204.20 $\mu$ H
Transmitter coil internal resistance ( $R_t$ )	0.4 $\Omega$
Receiver coil turns ( $n_r$ )	30 (3 layers)
Receiver capacitance ( $C_{ra}$ )	23.43, 0.9423~2.617 nF
Receiver capacitances ( $C_{rb}, C_{rc}$ )	8.39~23.30, 28.23 nF
Receiver coil inductances ( $L_{ra}, L_{rb}, L_{rc}$ )	147.13, 148.76, 148.21 $\mu$ H
Receiver coil internal resistance ( $R_{rk}$ )	0.2 $\Omega$
Mutual inductances ( $M_{t,a}, M_{t,b}, M_{t,c}$ )	10.95, 11.33, 11.17 $\mu$ H
Energy-on-demand frequency ( $f_b$ )	77.81~142.48 kHz
Output filter capacitance ( $C_k$ )	47 $\mu$ F
Smoothing inductance ( $L_i$ )	5.0 $\mu$ H

generate a 2-D discrete-time chaotic series as given by

$$\begin{cases} \xi_{f-i+1} = \xi_{d-i} + 1 - A_f \xi_{f-i}^2, & A_f \in [1.0, 1.5], A_d = 0.3 \\ \xi_{d-i+1} = A_d \xi_{f-i} \end{cases} \quad (17)$$

where  $\xi_{f-i}$  and  $\xi_{d-i}$  denote the chaotic sequences of the frequency and its duration from energy-on-demand, respectively;  $A_f$  and  $A_d$  are the corresponding bifurcation parameters. To produce the desired random-like but bounded security series ( $\xi_f, \xi_d$ ) for the energy-on-demand,  $A_f = 1.4$  is selected [21]. Hence, the chaotic security keys  $\gamma_i$  and  $\beta_i$  can be expressed as

$$\begin{cases} \gamma_i = a_\gamma + b_\gamma \xi_{f-i}, & 0 < 1.5 b_\gamma < a_\gamma \\ \beta_i = a_\beta + b_\beta \xi_{d-i}, & 0 < 0.4 b_\beta < a_\beta. \end{cases} \quad (18)$$

Consequently, the discrete energy-on-demand 2-D FDC is generated as  $(\gamma_i \omega_0, \beta_i D_0)$ . Generally,  $\omega_0$  and  $D_0$  can be arbitrarily designed based on the power level, transmission distance, and security requirements. Accordingly, the authorized receiver proactively adjusts its matched capacitor as

$$C_{rb} \left( \sum_{q=1}^{q=i} (\beta_i D_0) \right) = \frac{1}{r_i^2} \frac{1}{\omega_0^2 L_{rb}}. \quad (19)$$

The frequency and its duration from the authorized energy-on-demand can be chaotically varied. Generally, considering the wireless energy security, the frequency range for energy-on-demand should be from the lowest value to two or three times higher value, such as varying from 75 to 150 kHz or 225 kHz. Also, the wider the frequency range, the stronger the security performance can be resulted. With the informed security key, the quasi-resonant transmitter can self-adaptively attune its switching frequency to synchronize the authorized energy-on-demand. Finally, the encoded energy packages can only be decoded and picked up by those authorized receivers.

#### IV. RESULTS AND VERIFICATIONS

To illustrate the feasibility of proposed energy-on-demand MQRC-WPT system, finite element analysis (FEA) and system simulation are performed. Its design specifications and parameters are listed in Table I. For ensuring the wireless energy security and maximizing the transmission efficiency, the authorized

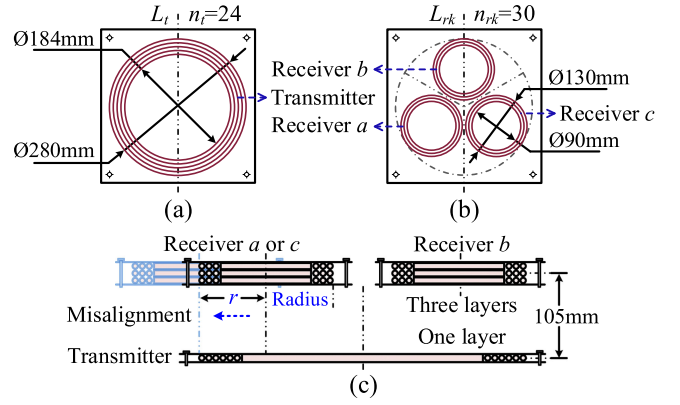


Fig. 7. Geometries of WPT coils. (a) Transmitter coil. (b) Receiver coils. (c) Displacement and misalignment.

energy-on-demand should elude the operating frequencies of those unauthorized receivers. Hence, the matched capacitances of the authorized receiver  $b$  and the unauthorized receivers  $a$  and  $c$  are respectively designed with the range of 8.39~23.30 nF, 23.43 nF, and 28.23 nF for the fundamental energy-on-demand under the SF-WPT, while those of the authorized receivers  $b$  and  $a$  are redesigned with the ranges of 8.39~23.30 nF and 0.9423~2.617 nF for the fundamental and 3rd harmonic energy-on-demands under the MF-WPT, respectively. The switching frequency can flexibly vary, thus generating the 1st and 3rd harmonic wireless powers for the arbitrary authorized energy-on-demand. The coil geometries are shown in Fig. 7, where each receiver can possibly conduct energy-on-demand to pick up wireless power. The prototype is to simulate a universal charging pad for consumer electronics or multiobjective WPT applications desiring high WPT-standard compatibility and wireless energy security.

#### A. Simulation Results

First, Fig. 8 depicts the electromagnetic field distributions among the WPT coils under the SF-WPT and MF-WPT. Since the magnetic field analysis in JMAG cannot simultaneously conduct multifrequency FEA, the MF-WPT is simulated by setting the 1st and 3rd harmonic separately in one current source. Whichever mode the proposed system operates at, Fig. 8(a)–(c) shows that the proposed energy-on-demand scheme effectively builds up the desired flux pipe, and thus almost all of the flux lines are bound up through the authorized receiver coil in which the current density is much higher than those in the unauthorized ones. Under the SF-WPT in Fig. 8(a), only the receiver coil  $b$  is authorized to pick up the single-frequency wireless power. Under the MF-WPT, two different receiver coils: coil  $b$  in Fig. 8(b) and coil  $a$  in Fig. 8(c), can simultaneously be authorized to harvest the 1st and 3rd harmonic wireless powers, respectively. Under the SF-WPT and MF-WPT, the flux densities along the middle parallel plane are plotted in Fig. 8(d)–(f), where their flux densities can reach up to 0.244, 0.196, and 0.187 mT, respectively.

Second, Fig. 9(a) shows the simulation waveforms under the MF-WPT. Notedly, both the transmitter and the authorized

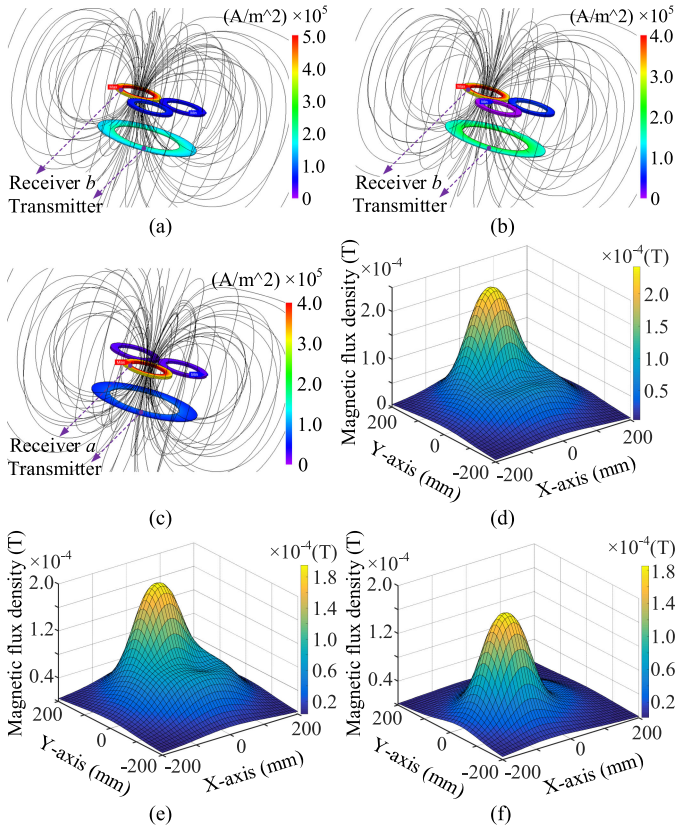


Fig. 8. Electromagnetic field distributions. (a) Flux lines and current densities under SF-WPT. (b) Flux lines and current densities under MF-WPT (1st). (c) Flux lines and current densities under MF-WPT (3rd). (d) Flux density along middle parallel plane under SF-WPT. (e) Flux density along middle parallel plane under MF-WPT (1st). (f) Flux density along middle parallel plane under MF-WPT (3rd).

receivers operate at their respective resonances. Although their resonant frequencies are different, the driving signal can attune the transmitter's equivalent operating frequency to synchronize the authorized arbitrary energy-on-demand frequency within an encryption range. At an exemplified energy-on-demand frequency, the transmitter current  $i_t$  resonates at its innate frequency which differs from the resonant frequencies of the receiver currents  $i_{rb}$  (fundamental) and  $i_{ra}$  (3rd harmonic). By controlling the frequency of driving signal  $u_{gS1}$ , the equivalent fundamental and 3rd harmonic frequencies of transmitter current  $i_t$  can be attuned to equal those of the authorized receiver currents  $i_{rb}$  and  $i_{ra}$ , respectively. With a controllable switching frequency, the transmitter can simultaneously energize the two authorized receivers  $b$  and  $a$  by satisfying their energy-on-demand frequencies. Also, two authorized receivers can equally harvest wireless power and generate approximately the same output voltages, namely 4.52 and 4.47 V. Under the MF-WPT, there is  $\omega_b^{(3)} = 3\omega_b^{(1)}$ . When the transmitter switches at the operating point  $(f_b, 0.333)$ , as labeled in Fig. 5(a), where  $i_t^{(1)} = 3i_t^{(3)}$ , the authorized receivers  $b$  and  $a$  can generate the same induced EMFs as  $j\omega_b^{(1)} M_{t,b} i_t^{(1)} = j\omega_b^{(3)} M_{t,a} i_t^{(3)}$  with the same mutual inductances  $M_{t,k}$ . With the same loads, the two authorized receivers will generate the same resonant currents which will

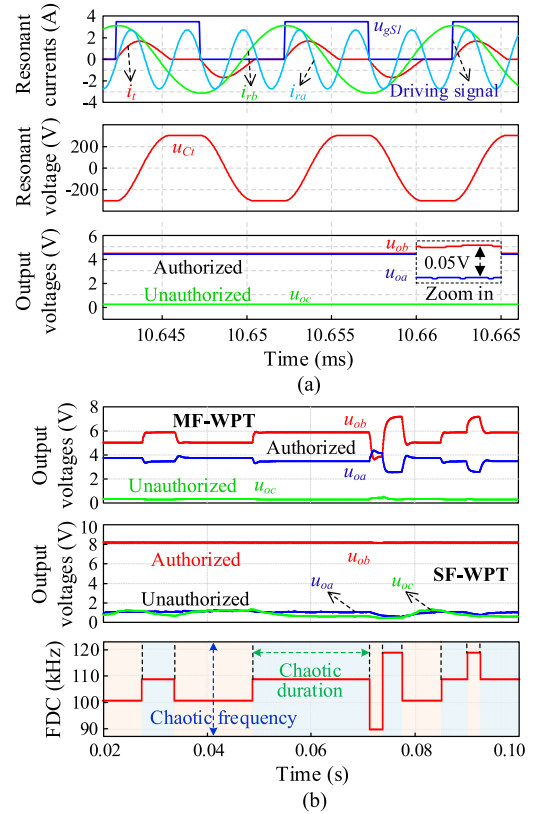


Fig. 9. Simulation waveforms. (a) MF-WPT. (b) Energy-on-demand.

contribute to almost the same flux densities under the receivers and thus the nearly same output voltages. Actually, these output voltages and the power distribution can be artificially set by choosing an appropriate energy-on-demand frequency. By applying the proposed 2-D FDC algorithm, the receivers' output voltages are 5.04, 3.76, and 0.33 V under the MF-WPT, while they are 8.2, 1.06, and 0.92 V under the SF-WPT, as shown in Fig. 9(b). The receivers  $b$  and  $a$  can be simultaneously or independently authorized to conduct energy-on-demand, thus harvesting the fundamental and/or 3rd harmonic wireless powers, respectively, but the unauthorized receiver  $c$  fails due to the lack of security keys. Also, the operating frequency and its duration are both chaotically encrypted in the proposed 2-D chaotic energy-on-demand. Namely, the magnitudes corresponding to the variable operating frequencies are chaotically encrypted, while the widths corresponding to the duration time of each frequency are also chaotically encrypted, thus forming the so-called 2-D FDC. It confirms that the proposed MQRC-WPT scheme can self-adapt to the authorized energy-on-demand and effectively prevent energy theft or leakage.

Finally, some key characteristics of the receiving power and transmission efficiency are simulated, as shown in Fig. 10. With the 2- $\Omega$  load  $R_{Lk}$ , Fig. 10(a) and (b) depicts the increasing trends of the receiving power and transmission efficiency with the increasing smoothing inductance, respectively. As noted, the receiving power is significantly enhanced by introducing the smoothing inductor, an improvement of 82.2% with the use of

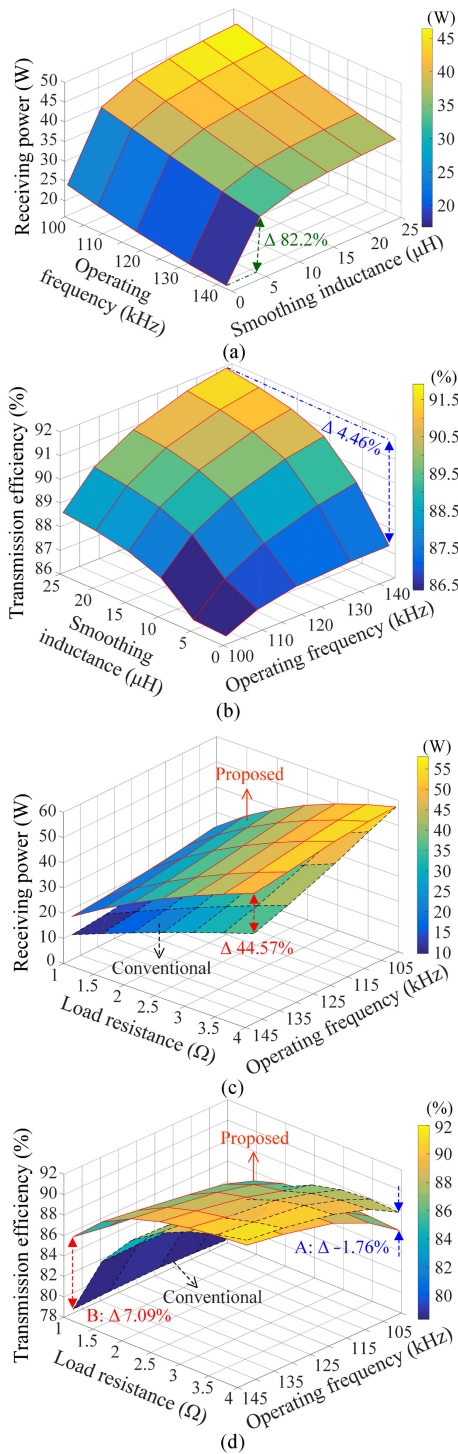


Fig. 10. Simulation characteristics. (a) Receiving power versus smoothing inductance. (b) Transmission efficiency versus smoothing inductance. (c) Receiving power versus load. (d) Transmission efficiency versus load.

5- $\mu\text{H}$  smoothing inductance. Moreover, the increase of transmission efficiency can reach up to 4.46% with the 25- $\mu\text{H}$  smoothing inductance. With the 5- $\mu\text{H}$  smoothing inductance, Fig. 10(c) and (d) depicts the receiving power and the transmission efficiency with the increasing load resistance, respectively. The proposed MQRC-WPT scheme can harvest much higher power than the

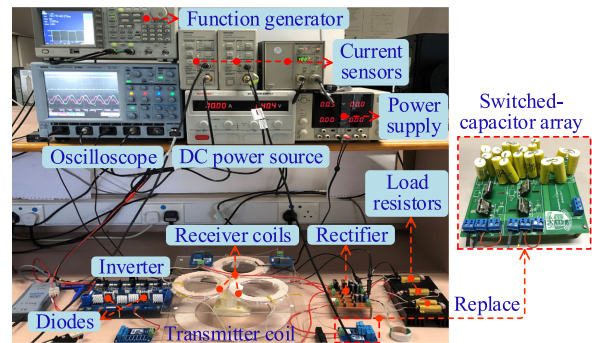


Fig. 11. Experimental setup.

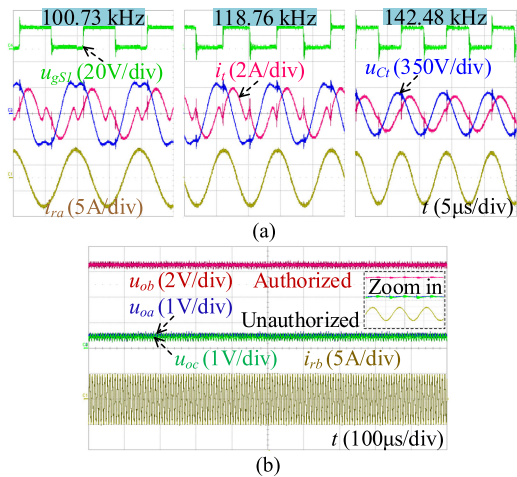


Fig. 12. Measured waveforms of MQRC-WPT system under SF-WPT. (a) Driving signal and resonances. (b) Output voltages.

conventional scheme, and the corresponding improvement can reach up to 44.57%. Although the transmission efficiency in the proposed scheme is slightly lower by 1.76% at some operating points as compared with that in the conventional one, it is significantly improved by 7.09% especially in the low output power level, and is more uniform over the variations of load resistance and operating frequency. Moreover, the characteristics of Fig. 10(c) and (d) can be further improved by increasing the smoothing inductance, as depicted in Fig. 10(a) and (b).

## B. Experimental Results

To assess the feasibility of the proposed energy-on-demand MQRC-WPT scheme, a prototype is built for experimental verification, as shown in Fig. 11. Under the SF-WPT, each receiver *a*, *b*, or *c* adopts a fixed matched capacitor, and only the authorized receiver *b* resonates at the exemplified operating frequency. As for dynamic energy-on-demand, the authorized receiver *b* uses a switched-capacitor array to replace its fixed capacitor, thus generating dynamic energy-on-demand. In order to verify various power distributions under the MF-WPT, the matched capacitor is redesigned as another value in the newly authorized receiver *a* to harvest harmonic wireless power.

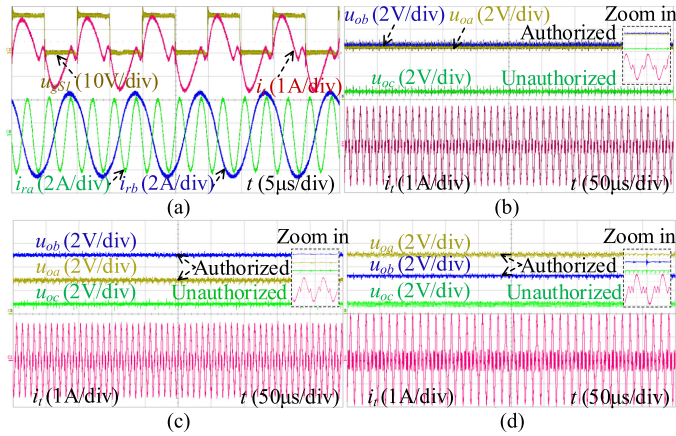


Fig. 13. Measured waveforms of MQRC-WPT system under MF-WPT. (a) Driving signal and resonant currents. (b) Output voltages ( $u_{ob} \approx u_{oa}$ ) and transmitter current. (c) Output voltages ( $u_{ob} > u_{oa}$ ) and transmitter current. (d) Output voltages ( $u_{ob} < u_{oa}$ ) and transmitter current.

First, Fig. 12 shows the measured waveforms of the driving signal and resonances as well as output voltages at three typical energy-on-demand frequencies under the SF-WPT. Both the transmitter and the authorized receiver resonate at their respective inherent resonances. Due to the inevitable reverse recovery of nonideal power devices, there are slight ripples in the transmitter current and voltage during the dead zone, instead of keeping constant as compared with the simulated waveforms in Fig. 9(a). Nevertheless, by symmetrically separating the positive and negative sinusoidal half-cycles of the transmitter current, the driving signal can successfully attune the equivalent operating frequency of the quasi-resonant transmitter to synchronize with the authorized receiver's energy-on-demand frequency. Thus, the switched-capacitorless quasi-resonant transmitter can achieve continuous frequency regulation to self-adapt the authorized receiver's arbitrary energy-on-demand.

Second, Fig. 13 shows the measured waveforms of the proposed energy-on-demand MQRC-WPT system under the MF-WPT, which utilizes the 1st (100.73 kHz) and 3rd harmonic (302.19 kHz) components as the outputs. The measured waveforms of driving signal, transmitter resonant current, and two authorized receivers' resonant currents are shown in Fig. 13(a), where the switching frequency equals the fundamental frequency of the energy-on-demand. Compared with the simulated waveforms in Fig. 9(b), although the transmitter current slightly fluctuates during the dead zone, the 1st and 3rd harmonic currents can synchronously excite the  $b$ th and  $a$ th authorized receivers, respectively. Fig. 13(b) shows the measured transmitter current as well as output voltages of the authorized and unauthorized receivers. Notedly, the  $a$ th and  $b$ th receivers can simultaneously pick up the 1st and 3rd harmonic wireless powers, and generate the approximately equal output voltages of 4.677 and 4.45 V, respectively, while the  $c$ th unauthorized receiver can pick and generate only an insignificant value, which well agrees with the simulated results in Fig. 9(b). Various power distributions between the 1st and 3rd harmonic components can be realized by regulating the operating frequency. At different

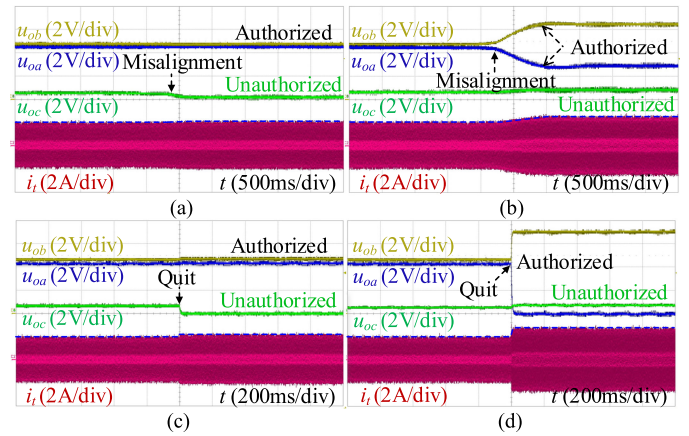


Fig. 14. Dynamic characteristics of wireless energy-on-demand system. (a) Unauthorized receiver misalignment. (b) Authorized receiver misalignment. (c) Unauthorized receiver quit. (d) Authorized receiver quit.

energy-on-demand operating frequencies of 114.36 and 85.49 kHz, different power distributions between the 1st and 3rd harmonic components are shown in Fig. 13(c) and (d), respectively. The various output voltage variations ( $u_{ob} > u_{oa}$  and  $u_{ob} < u_{oa}$ ) demonstrate that the 1st wireless powers harvested by the authorized receiver  $b$  differ from the 3rd ones harvested by the authorized receiver  $a$ .

Furthermore, the dynamic characteristics are measured, as shown in Fig. 14(a) and (b), in which only one unauthorized receiver or only one authorized receiver is misaligned by up to a radius  $r$ , as depicted in Fig. 7(c). Due to the insignificant change in the total reflected impedance, Fig. 14(a) shows that the proposed MQRC-WPT system is nearly impervious to this slightly beneficial scenario of the unauthorized receiver  $c$  misalignment. When the authorized receiver  $a$  is misaligned in Fig. 14(b), the transmitter current slightly increases. As a result, the wireless powers harvested by the authorized receivers  $a$  and  $b$  accordingly decreases and increases, respectively. It indicates that the quasi-resonant operation in the transmitter can competently achieve the proposed energy-on-demand WPT scheme in this adverse scenario. Inevitably, the proposed MQRC-WPT system performance will be slightly degraded when a serious misalignment happens only in the authorized receiver. Meanwhile, the other dynamic characteristics are measured, as shown in Fig. 14(c) and (d), in which only one unauthorized receiver, or only one authorized receiver quits. Similarly, Fig. 14(c) shows that the proposed MQRC-WPT system is nearly impervious to this beneficial scenario where the unauthorized receiver  $c$  quits. When the authorized receiver  $a$  quits in Fig. 14(d), the transmitter current suddenly increases. As a result, the wireless powers harvested by the remaining authorized receiver  $b$  accordingly increases. It confirms that the proposed system can still satisfy the authorized wireless energy-on-demand in this greatly adverse scenario. These dynamic characteristics indicate that the proposed MQRC-WPT system can effectively keep a good tolerance to these scenarios even when the authorized receiver suddenly quits.

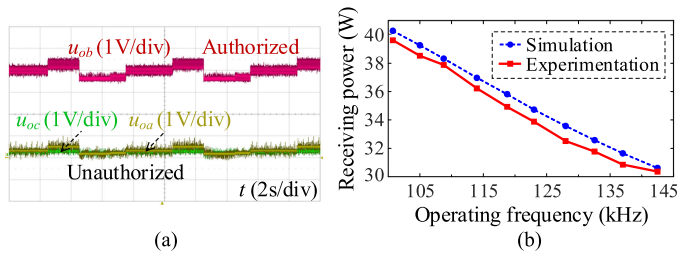


Fig. 15. Measured waveforms of proposed WPT system. (a) Energy-on-demand using 2-D FDC. (b) Simulated and measured characteristics.

TABLE II  
SYSTEM CHARACTERISTIC COMPARISONS

Items	Conventional MRC	Proposed MQRC
SF-WPT	Yes	Yes
MF-WPT	No	Yes
Adjustment continuity	No	Yes
Transmission efficiency	82.32%	84.86%

Finally, in order to online tune the compensation of the authorized receiver, the switched-capacitor array is controlled by a digital signal processor (TMS320F28335) to provide the desired automatic capacitance adjustment. In Fig. 15(a), both the voltage levels and their widths, controlled by the chaotic 2-D FDC sequence, indicate the chaotic variations of the operating frequency and its duration in the proposed energy-on-demand. Moreover, the characteristic of receiving power versus energy-on-demand frequency is measured and compared with its simulated one under the same input, as shown in Fig. 15(b). Although the measured receiving power is slightly lower than the simulated one which is due to the inevitable power loss along switches, diodes, lines, and contacts, it confirms the power transmission enhancement by introducing a smoothing inductor. Besides, the system characteristic comparisons between the MRC-WPT and MQRC-WPT at 142.48 kHz are experimentally verified as listed in Table II. The measured transmission efficiency is 84.86%, slightly lower than its theoretical value of 88.62%. Their slight difference is due to the slight parameter deviations and the inevitable power losses along the lines and contacts. Also, the transmission efficiency of the proposed scheme is confirmed to be higher than those using the conventional one. Due to the inevitable power losses along the matched capacitors, lines, contacts, and rectifiers, the measured system efficiency of 70.06% is lower than the theoretical coil-to-coil efficiency of 92.29% which has only considered the coil losses. Nevertheless, it can be readily improved by decreasing the ratio of the transmission distance to the receiver coil radius or by increasing the power level. Meanwhile, when the number of unauthorized receivers increases, there is only a slight decrease in the measured system efficiencies. For instance, it decreases by 0.53% and 0.94% for one and two unauthorized receivers, respectively.

### C. Discussion

Similar to the information security, wireless energy security deserves to be seriously concerned. Illegal users may detect

and track the fixed operating frequency of the SF-WPT, thus readily stealing wireless energy and significantly deteriorating system performance. The one-to-many WPT scenarios, such as the electric vehicle charging roadways or parking lots [9], automatic wireless charging machines, and public multifunctional wireless charging desks, inevitably suffer from a crucial risk of wireless energy theft or leakage. The authorization of wireless charging should be properly granted to paid users, while the unpaid charging is prohibited. This article focuses on improving the wireless energy security and proposes an energy-on-demand SF-WPT or MF-WPT scheme using the 2-D chaotic encryption. Its main novelties and advantages include: 1) transferring the initiative to the authorized receiver; 2) guaranteeing wireless energy security; 3) enabling high-efficiency power transmission without energy theft or leakage; 4) assisting the transmitter with continuous frequency regulation; and 5) improving the WPT standard compatibility. Although this variable-frequency encryption may slightly reduce the system efficiency, wireless energy theft or leakage will cause more significant power and efficiency losses.

The exemplified frequency range of 77.8–142.5 kHz can be flexibly redesigned or widen for various WPT-based applications desiring the wireless energy security. More importantly, the relevant WPT standards will move forward to further standardize the frequency range for energy encryption. Although the current power level for implementing the proposed system is several tens of watts, the system can readily be designed to operate at higher power levels such as several kilowatts for dynamically charging electric vehicles over electrified roadways.

In the proposed wireless energy-on-demand, it usually involves high-frequency fast switching for maintaining high-efficiency power transmission. Such fast switching may inevitably generate the spurious spectrum components, which will interfere with other radio systems. Besides, these generated spurious components may also overlap with the device's own receiving band, causing own receiver desensitization [22]. Nevertheless, in the proposed system, the magnitudes of spurious components are very low due to their very large interband gap between the switching frequency (up to 300 kHz) and the radio frequency (2.4 GHz or over). In fact, the frequency-encrypted energy-on-demand can be essentially deemed as a chaotically frequency-hopping technique [23], which can inherently suppress the spurious spectrum components and thus reduce the electromagnetic interference on other radio systems.

## V. CONCLUSION

This article mainly focuses on improving the wireless energy security and the WPT standard compatibility, and thus it conceives an energy-on-demand SF-WPT or MF-WPT scheme using the 2-D chaotic encryption. In particular, the novelties of this article can be summarized as follows.

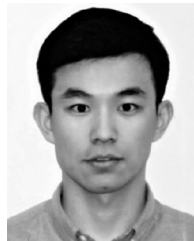
- 1) The energy-on-demand technology transfers the initiative to the authorized receiver to generate the security keys of 2-D FDC, which enables high-efficiency power transmission without energy theft or leakage.

- 2) To prevent the illegal frequency tracking, the 2-D FDC chaotically encrypts both the operating frequency and its duration. The multiobjective WPT systems possess better energy security performance.
- 3) In the MQRC-WPT, the quasi-resonant transmitter contributes to a continuous frequency regulation for flexibly self-adapting the customized chaotic energy-on-demand. Also, it can be further configured to a synchronous MF-WPT mode for improving the WPT standard compatibility.
- 4) The MQRC-WPT, incorporated with an output smoothing inductor, can provide the power transmission enhancement over the conventional one while improving the transmission efficiency especially during the low power level.

Both simulation and experimental results have been given to verify the feasibility of proposed energy-on-demand MQRC-WPT system. The energy-on-demand MQRC-WPT technology is promising for various multi-objective WPT applications desiring high WPT-standard compatibility and energy security.

#### REFERENCES

- [1] A. Kamineni, M. J. Neath, G. A. Covic, and J. T. Boys, "A mistuning-tolerant and controllable power supply for roadway wireless power systems," *IEEE Trans. Power Electron.*, vol. 32, no. 9, pp. 6689–6699, Sep. 2017.
- [2] T. Kan, R. Mai, P. P. Mercier, and C. C. Mi, "Design and analysis of a three-phase wireless charging system for lightweight autonomous underwater vehicles," *IEEE Trans. Power Electron.*, vol. 33, no. 8, pp. 6622–6632, Aug. 2018.
- [3] X. Dai, J. Jiang, and J. Wu, "Charging area determining and power enhancement method for multiexcitation unit configuration of wirelessly dynamic charging EV system," *IEEE Trans. Ind. Electron.*, vol. 66, no. 5, pp. 4086–4096, May 2019.
- [4] S. Y. Jeong, H. G. Kwak, G. C. Jang, S. Y. Choi, and C. T. Rim, "Dual-purpose nonoverlapping coil sets as metal object and vehicle position detections for wireless stationary EV chargers," *IEEE Trans. Power Electron.*, vol. 33, no. 9, pp. 7387–7397, Sep. 2018.
- [5] C. Jiang, K. T. Chau, W. Liu, C. Liu, W. Han, and W. H. Lam, "An LCC compensated multiple-frequency wireless motor system," *IEEE Trans. Ind. Inform.*, vol. 15, no. 11, pp. 6023–6034, Nov. 2019.
- [6] Y. Li *et al.*, "Analysis, design and experimental verification of a mixed high order compensations-based WPT system with constant current outputs for driving multistring LEDs," *IEEE Trans. Ind. Electron.*, vol. 67, no. 1, pp. 203–213, Jan. 2020.
- [7] C. C. Mi, G. Bujja, S. Y. Choi, and C. T. Rim, "Modern advances in wireless power transfer systems for roadway powered electric vehicles," *IEEE Trans. Ind. Electron.*, vol. 63, no. 10, pp. 6533–6545, Oct. 2016.
- [8] Z. Zhang, H. Pang, A. Georgiadis, and C. Cecati, "Wireless power transfer—An overview," *IEEE Trans. Ind. Electron.*, vol. 66, no. 2, pp. 1044–1058, Feb. 2019.
- [9] Z. Zhang, K. T. Chau, C. Qiu, and C. Liu, "Energy encryption for wireless power transfer," *IEEE Trans. Power Electron.*, vol. 30, no. 9, pp. 5237–5246, Sep. 2015.
- [10] J. Tian and A. P. Hu, "A dc-voltage-controlled variable capacitor for stabilizing the ZVS frequency of a resonant converter for wireless power transfer," *IEEE Trans. Power Electron.*, vol. 32, no. 3, pp. 2312–2318, Mar. 2017.
- [11] Q. C. Zhong and Y. Zeng, "Control of inverters via a virtual capacitor to achieve capacitive output impedance," *IEEE Trans. Power Electron.*, vol. 29, no. 10, pp. 5568–5578, Oct. 2014.
- [12] S. Yan, M. Wang, T. Yang, S. Tan, B. Chaudhuri, and S. Y. R. Hui, "Achieving multiple functions of three-phase electric springs in unbalanced three-phase power systems using the instantaneous power theory," *IEEE Trans. Power Electron.*, vol. 33, no. 7, pp. 5784–5795, Jul. 2018.
- [13] F. Liu, Y. Yang, Z. Ding, X. Chen, and R. M. Kennel, "A multi-frequency superposition methodology to achieve high efficiency and targeted power distribution for multi-load MCR WPT system," *IEEE Trans. Power Electron.*, vol. 33, no. 10, pp. 9005–9016, Oct. 2018.
- [14] C. Zhao and D. Costinett, "GaN-based dual-mode wireless power transfer using multifrequency programmed pulse width modulation," *IEEE Trans. Ind. Electron.*, vol. 64, no. 11, pp. 9165–9176, Nov. 2017.
- [15] Z. Pantic, K. Lee, and S. M. Lukic, "Multifrequency inductive power transfer," *IEEE Trans. Power Electron.*, vol. 29, no. 11, pp. 5995–6005, Nov. 2014.
- [16] Y. Zhang, T. Lu, Z. Zhao, F. He, K. Chen, and L. Yuan, "Selective wireless power transfer to multiple loads using receivers of different resonant frequencies," *IEEE Trans. Power Electron.*, vol. 30, no. 11, pp. 6001–6005, Nov. 2015.
- [17] W. Liu, J. Zhang, and R. Chen, "Modelling and control of a novel zero-current-switching inverter with sinusoidal current output," *IET Power Electron.*, vol. 9, no. 11, pp. 2205–2215, Sep. 2016.
- [18] S. Samanta and A. K. Rathore, "A new current-fed CLC transmitter and LC receiver topology for inductive wireless power transfer application: analysis, design, and experimental results," *IEEE Trans. Transport. Electrific.*, vol. 1, no. 4, pp. 357–368, Dec. 2015.
- [19] X. Tan and X. Ruan, "Optimal design of DCM LCC resonant converter with inductive filter based on mode boundary map," *IEEE Trans. Power Electron.*, vol. 30, no. 8, pp. 4144–4155, Aug. 2015.
- [20] W. Liu, K. T. Chau, C. H. T. Lee, C. Jiang, and W. Han, "A switched-capacitorless energy-encrypted transmitter for roadway-charging electric vehicles," *IEEE Trans. Magn.*, vol. 54, no. 11, pp. 1–6, Nov. 2018.
- [21] M. Hénon, "A two-dimensional mapping with a strange attractor," *Commun. Math. Phys.*, vol. 50, no. 1, pp. 69–77, Feb. 1976.
- [22] M. Abdelaziz, L. Anttila, C. Tarver, K. Li, J. R. Cavallaro, and M. Valkama, "Low-complexity subband digital predistortion for spurious emission suppression in noncontiguous spectrum access," *IEEE Trans. Microw. Theory Tech.*, vol. 64, no. 11, pp. 3501–3517, Nov. 2016.
- [23] J. Chen, P. Liu, Y. Hung, H. Yang, and Y. E. Chen, "A spur-reduced multi-mode power-level tracking power amplifier using a frequency-hopping dc–dc converter," *IEEE Trans. Microw. Theory Tech.*, vol. 58, no. 5, pp. 1333–1338, May 2010.



**Wei Liu** (Student Member, IEEE) received the B.Eng. degree in electrical engineering and automation and the M.Eng. degree in electrical engineering from the China University of Petroleum (East China), Qingdao, China, in 2014 and 2017, respectively. He is currently working toward the Ph.D. degree in electrical and electronic engineering with the Department of Electrical and Electronic Engineering, The University of Hong Kong, Hong Kong.

He was a Visiting Researcher with the Nanyang Technological University, Singapore, in 2019. His research interests include power electronics, wireless power transfer techniques, and electric vehicle technologies.



**K. T. Chau** (Fellow, IEEE) received the B.Sc. (Eng.), M.Phil., and Ph.D. degrees in electrical and electronic engineering from The University of Hong Kong, Hong Kong, in 1988, 1991, and 1993, respectively.

Since 1995, he has been with The University of Hong Kong, where he is currently a Professor with the Department of Electrical and Electronic Engineering. He has authored and coauthored nine books and more than 300 journal papers. His research interests include electric and hybrid vehicles, power electronics and drives, and renewable energies.

Prof. Chau was the recipient of the Changjiang Chair Professorship from the Ministry of Education, China, and the Environmental Excellence in Transportation Award for Education, Training, and Public Awareness from the Society of Automotive Engineers International. He is a Fellow of the Institution of Engineering and Technology (IET), U.K., and also of the Hong Kong Institution of Engineers. He is currently also a Co-editor of the *Journal of Asian Electric Vehicles*. He is a Chartered Engineer in Hong Kong.



**Christopher H. T. Lee** (Senior Member, IEEE) received the B.Eng. (first Class honors.) and Ph.D. degrees in electrical engineering from the Department of Electrical and Electronic Engineering, The University of Hong Kong, Hong Kong, in 2009 and 2016, respectively.

He is currently an Assistant Professor in power engineering with the Nanyang Technological University, Singapore, a Visiting Assistant Professor with the Massachusetts Institute of Technology, Cambridge, MA, USA, and an Honorary Assistant Professor in the *alma mater*. He has authored and coauthored one book, three book chapters, and about 70 referred papers. His research interests include electric machines and drives, renewable energies, and electric vehicle technologies.



**Chaoqiang Jiang** (Member, IEEE) received the B.Eng. and M.Eng. degrees in automation from Wuhan University, Wuhan, China, in 2012 and 2015, respectively, and the Ph.D. degree in electrical and electronic engineering from The University of Hong Kong, Hong Kong, in 2019.

He is currently a Postdoctoral Research Associate with the University of Cambridge, Cambridge, U.K. In 2019, he was a Visiting Researcher with the Nanyang Technological University, Singapore. His research interests include power electronics, wireless power transfer techniques, and electric vehicle technologies.



**Wei Han** (Student Member, IEEE) received the B.Eng. degree in electrical engineering and automation from Northeastern University, Shenyang, China, in 2014, and the M.Eng. degree in electrical and electronic engineering in 2015, from The University of Hong Kong, Hong Kong, where he is currently working toward the Ph.D. degree in electrical and electronic engineering with the Department of Electric and Electronic Engineering.

His research interests include wireless power transfer techniques, power electronics, and renewable energies.



**W. H. Lam** (Senior Member, IEEE) was born in Hong Kong. He received the B.Sc. degree in computer and communication engineering from the University of Essex, Essex, U.K., in 1983, the M.Sc. degree in telecommunication engineering from the Imperial College, University of London, London, U.K., in 1984, and the Ph.D. degree in digital mobile radio communications from the University of Southampton, Southampton, U.K., in 1988.

In 1991, he joined the Department of Electrical and Electronic Engineering, University of Hong Kong, Hong Kong. He has authored and coauthored more than 70 technical publications in the field of digital cellular mobile radio communications and the intelligent transport systems (ITS). His current research interest includes the next generation digital mobile radio and spread spectrum communications systems, ITS, and power electronics and drives.

Dr. Lam was the recipient of the SERC CASE Award from the University of Southampton. He was the Chairman and Organizer of a series of regional conferences on mobile radio communications and a Distinguished Speaker and Chairperson at several international conferences and meetings.